Available online at www.sciencedirect.com
ScienceDirect
Physica A 373 (2007) 737–746
PHYSICA A
www.elsevier.com/locate/physa

Fractal and topological dynamics for the analysis of paleoclimatic records

L. Karimova[a], Y. Kuandykov[a], N. Makarenko[a], M.M. Novak[b,*], S. Helama[c]

[a]*Institute of Mathematics, Almaty, Kazakhstan*
[b]*Faculty of CISM, Kingston University, Surrey KT1 2EE, England*
[c]*Department of Geology, University of Helsinki, PO Box 64, FIN-00014, Finland*

Received 8 March 2006; received in revised form 10 March 2006
Available online 24 May 2006

Abstract

The paper focuses on the investigation of time series of paleoclimatic proxy records of Finland's temperature and the ratio of oxygen isotope in ice cores of Greenland. Joint study of these records should improve the understanding of the climatic variability over the entire North Atlantic sector. Paleoclimatic proxy records are analyzed with the help of multifractal formalism, wavelet analysis and topological dynamics methods to reveal scaling features as well as their nonlinear dynamics and interrelationship.
© 2006 Elsevier B.V. All rights reserved.

Keywords: Multifractal formalism; Scaling; Paleoclimatic records

1. Introduction

Variability of natural processes over the North Atlantic region, including coupled ocean-atmosphere system, has strong climatic impact from eastern seaboard of the United States to Siberia, from the Arctic to the subtropical Atlantic [1]. Variations in the climate over Greenland and Northern Europe are likewise largely dictated by this natural circulation system [2]. Understanding the connections of the climate perturbations in different regions requires long time series of paleoclimatic proxy records. The term "proxy records" means that information is embedded in natural carriers, such as isotopes in ice cores in Greenland and tree-ring chronologies of living and subfossil wood in North-West Europe. These have stored the records of temperature variability within the North Atlantic sector. Investigation combining these records should improve the understanding of the climatic variability over the entire North Atlantic region.

To study past climates and associated environmental changes, the analysis of ice-core drilling was carried out. Ice cores offer great potential for such studies, because each annual layer deposited on polar ice sheets is assumed to preserve all components that were deposited with the snow in the year the layer was formed [3]. The isotopic composition of the ice yields information about the temperature; the dust informs about

*Corresponding author.
E-mail address: novak@kingston.ac.uk (M.M. Novak).

0378-4371/$ - see front matter © 2006 Elsevier B.V. All rights reserved.
doi:10.1016/j.physa.2006.04.061

storminess and source efficiency; the air bubbles reflect the greenhouse gases in the atmosphere; the acidity contains details related to volcanic eruptions in the northern hemisphere; chemical traces are the products of various processes on land, in the sea, and in the atmosphere at the time of formation of the ice [3]. Several ice cores, reaching bedrock, have been drilled through the Greenland ice sheet during the joint European Greenland Ice Core Project (GRIP) and various isotopic, chemical, and physical properties of the core have been measured. Ice core based proxy record is also available in the Greenland Ice Sheet Project (GISP 2) δ^{18}O data set, measured at the University of Washington's Quaternary isotope laboratory.[1]

To obtain information about the temperature, the stable isotope ratio, $^{18}O/^{16}O$, provides the main reference parameter, since its variability is determined mainly by the cloud temperature at the moment of snow formation and thus has direct climatic relevance, assuming unchanged temperature and humidity at the original moisture source areas [3]. On the Greenland ice sheet, the present mean annual δ^{18}O of the snow is related closely to the mean annual surface temperature, T, in °C, through the formula

$$\delta^{18}\mathrm{O} = 0.67 * T - 13.7‰,$$

where δ^{18}O is the per mil deviation of $^{18}O/^{16}O$ ratio in a sample from the $^{18}O/^{16}O$ value in standard mean ocean water (SMOW). The temporal relationship between the δ^{18}O and the surface temperature T can be inferred by modelling the borehole temperature profile, based on a surface temperature history determined by a simple relation to the well-dated δ^{18}O profile.

While these records extend from the 1980s back 110977 years BP,[2] the focus will be on the last seven and a half millennia, due to particular emphasis on the comparison with the tree-ring data of the same length. The original time series δ^{18}O is not equidistant, and, moreover, it contains gaps. Consequently, we also use additional time series containing the equidistant GISP2 annual data δ^{18}O extended back to 1133 years BP and compare it with the tree-ring temperature data.

The present tree-ring dataset includes Scots pine (*Pinus sylvestris* L.) ring-width series from forest-limit region of northern Fennocandia, Finland and Norway. This regional chronology is a composite ring-width chronology of living tree and dead wood samples, from 1081 trees. The latter source comes from the logs lying on the ground as snags, and from the lake sediments where they have been preserved over the years. Collection and sampling of the trees were described in great detail by Eronen et al. [4,5]. At the moment, the chronology spans continuously over past 7.5 thousand years. Tree-ring widths were measured under light-microscope to the nearest 0.01 mm and carefully cross-dated using several numerical methods [6] along with visual comparison of tree-ring characteristics. In dendrochronological cross-dating the variations in ring-widths are first examined and then synchronized among all available samples from a given region. Covariation among tree-ring series ensures the absolute dating of each ring to the accuracy of 1 year. This is a synchronization of tree-ring series called cross-dating and it provides the annual dating control of examined characteristics [7].

Regional curve standardization (RCS) [8] was applied in dendrochronological growth trend removal process. This is a process called tree-ring standardization, it removes the non-climatic noise (mainly from tree ageing) from individual time series of ring-widths prior to chronology calculations. In RCS method one first realigns all available ring-width time series with their biological age to obtain an average tree ageing curve represented by the trees. As trees are rearranged according to their biological (cambial) age, no other factors than ageing are expected to be preserved in the averaged regional curve. This curve is then smoothed, and tree-ring indices are extracted from the curve as ratios. The method of RCS has been shown to reveal greater centennial-scale variability in resulting tree-ring chronology, compared to the earlier works using the similar tree-ring material but different tree-ring standardization [9].

Forest-limit Scots pine ring-widths are known to correlate significantly and positively with mid-summer temperatures in Northern Finland [10–12]. This relationship enabled [9] to reconstruct July temperatures using the RCS based tree-ring indices back to about 5500 BC. Calibration and verification procedures exhibit a degree of skill in reconstruction for the examined test periods.

[1]The data is now downloadable from http://www.ngdc.noaa.gov/paleo

[2]Before present.

In this paper we investigate long time series of palaeoclimatic proxy records with the help of multifractal formalism, wavelet analysis and topological dynamics methods to reveal scaling features as well as their nonlinear dynamics and mutual relationship.

In order to apply the above methodologies, it was necessary to construct a time series with a similar resolution. Because the Greenland ice-core record is not equidistant, its gaps were filled by means of the method of fractal interpolation [13], taking into account the discovered fractal characteristics of the time series. Proxy data are a result of interference of various processes existent in cosmos and on the Earth. Therefore, "climatic signals" are corrupted by noises of various type of unknown nature. We use data enhancement for noise reduction [14,15], which is applicable in most common situations. After preprocessing, we investigate interdependence of two time series of proxy indicators of climate fluctuations on large time scales. The first time series is the yearly average July temperature in North Lapland from 5510 BP to 1993 AD. From now on, this time series will be denoted by T. The second time series is the abundance ratio of oxygen isotope in ice cores of Greenland from 8065 BP to 1987 AD. This series will be denoted as ^{18}O.

2. Multifractal characteristics

Multifractal formalism [16–18] has proved to be a very useful technique in the study of both, measures and functions, deterministic as well as random. Multifractal analysis connects pointwise regularity of the function with a "size" of sets where regularity possesses some value. The function regularity may change abruptly from one point to the next. The pointwise regularity [19] is a positive real number $\alpha(x)$, which describes a certain smoothness of the graph of a function at point x. In general, let h be a nonnegative real number, $x_0 \in R$, a function $F(x) : R \to R$ is $C^h(x_0)$ if there exists $C>0,\ \delta>0$ and a polynomial $P(x)$ of the order smaller than h so that

$$\text{if } |x - x_0| \leqslant \delta, \quad |F(x) - P(x - x_0)| \leqslant C|x - x_0|^h,$$

then Hölder exponent of F at x_0 is $\alpha(x_0) = sup\{h : F \text{ is } C^h(x_0)\}$. Let

$$E_\alpha = \{x \in R : \alpha(x) = \alpha\}.$$

Then fine (Hausdorff) multifractal spectrum [16] is

$$f_H(\alpha) = dim_H E_\alpha,$$

where $dim_H E_\alpha$ is the Hausdorff dimension of the set E_α. Because dim_H of the set is never more than its box dimension, one can estimate it by counting the boxes (or intervals) over F, which increase roughly with the "right" Hölder exponent. For that, "grain" exponents are applied, which for binary partition looks like that

$$\alpha_k^{(n)} = -\frac{1}{n}\log_2 sup\{|F(s) - F(t)| : (k-1)2^{-n} \leqslant s \leqslant t \leqslant (k+2)2^{-n}\}.$$

Then the grain multifractal spectrum defined [20] as

$$f_g(\alpha) = \lim_{\varepsilon \to 0} \lim_{n \to \infty} sup \frac{\log N^{(n)}(\alpha, \varepsilon)}{n \log 2},$$

where $N^{(n)}(\alpha, \varepsilon) = \#\{k : |\alpha_k^{(n)} - \alpha| < \varepsilon\}$, gives "probabilistic" description of singularity structure of the function and is called the large deviation spectrum [21]. This spectrum can be calculated by the kernel method [22].

It is impossible to obtain numerical estimations of multifractal spectra directly from the mathematical definition, since they include several intricate limits. Therefore, one uses the definition of the spectrum based on "averaged quantities" extracted from observed signal. These values are called "structure functions" [19] and evaluated either by L^p modulus of continuity of F

$$S_q(l) = \int |F(x + l) - F(x)|^q \, dx$$

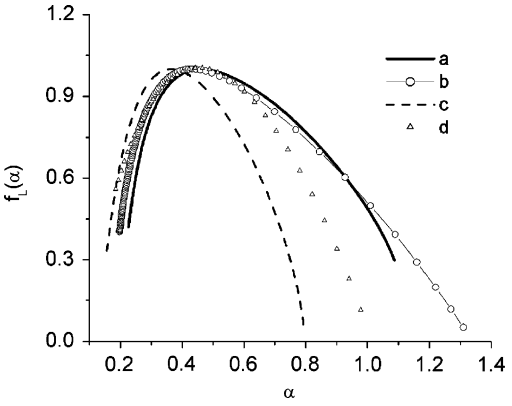

Fig. 1. Legendre $f(\alpha)$-spectra of decennial ^{18}O, namely, the short fragment (a) and time series with gaps reconstructed by linear interpolation (b). The curves (c) and (d) are the spectra of annual time series.

or

$$Z(a,q) = \int |C(a,b)|^q \, \mathrm{d}b,$$

where $C(a,b)$ is a wavelet transform of F, i.e.,

$$C(a,b) = \frac{1}{a}\int F(t)\psi\left(\frac{t-b}{a}\right)\mathrm{d}t.$$

Assume that the order of magnitude of $S_q(l)\sim|l|^{\zeta(q)}$, when $l \to 0$ and $Z(a,q)\sim a^{\eta(q)}$ in small box of size a, where $S\sim L$ means that

$$\lim(\log|S|)/(\log(|L|)) = 1.$$

Then multifractal spectrum is computed using the inverse Legendre transform of $\zeta(q)$ or $\eta(q)$ as

$$f_L(\alpha) = \inf_q(q\alpha - \zeta(q)) \quad \text{or} \quad f_L(\alpha) = \inf_q(q\alpha - \eta(q)).$$

In this paper we computed the large deviation spectrum $f_q(\alpha)$ and the Legendre spectrum $f_L(\alpha)$ using FracLab software.[3] Additionally, Legendre spectra were estimated by means of the method [18] of partition sum $Z_q(\varepsilon)\sim\sum p_i^q$ using our own program and the oscillation function $F(x)$ inside an ith ε-box as p_i.

The multifractal Legendre spectra of the time series ^{18}O are represented in Fig. 1. The multifractal spectrum of 10-year ^{18}O time series was computed for the fragment corresponding to 630–1990 BC (137 records), which is the longest one without gaps. Fig. 1 shows also the multifractal spectrum for the whole ^{18}O time series, where the gaps between available records were reconstructed using linear interpolation technique. Both of these spectra have a similar form, and their maxima approximately correspond to Hölder exponent equal to 0.5. The multifractal spectra of the annual data ^{18}O (curves "c" and "d") are characterized by the narrower $f_L(\alpha)$-curves. Nevertheless, their multifractal properties are confirmed by log–log behavior of partition sums $Z_q(\varepsilon)$ versus scale in Fig. 2. It should be noted, that Finland's temperature time series also demonstrates multifractal features. Consequently we apply fractal interpolation technique for recovering missed values in that data.

3. Fractal interpolation of data

In order to fill the gaps in the ^{18}O time series we used the fractal interpolation technique [13]. Roughly speaking, fractal interpolation can be considered as rescaling of known fragments of data, based on fractal properties of statistical self-similarity, and inserting them into intervals where data is absent. The method of

[3] http://fractales.inria.fr

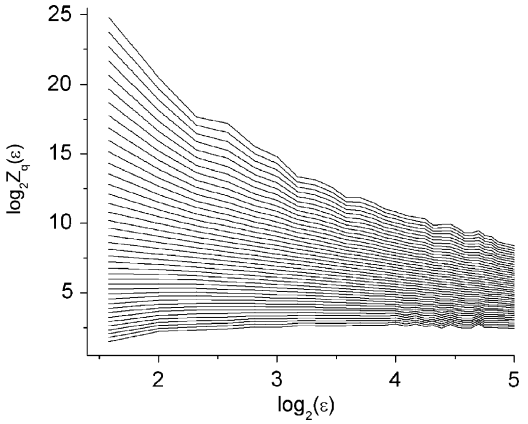

Fig. 2. The log–log behavior of partition sums $Z_q(\varepsilon)$ versus scale for the "d" curve of the Fig. 1.

fractal interpolation is optimal in the case when there is no prior information on data structure corresponding to the short scales, and the original time series exhibits fractal properties.

We pose the fractal interpolation problem with a set of input points $\{(x_i, y_i)\}_{i=0}^{N}$ with nodes $0 = x_0 < x_1 < \cdots < x_N = 1$ and ordinates $y_i = F_{app}(x_i) \in R$ assuming some continuous function $F_{app} : [0, 1] \to R$. Classically, if F_{app} is assumed smooth, then the input points are interpolated globally with a single polynomial of degree N, or piecewise with low-degree polynomials. An alternative assumption is that the interpolation function F_{app} is self-similar, and typically not smooth, but fractal. Such a function is called a *Fractal Interpolating Function* (FIF) [16]. Let $Gr(F_{app}) = \{(x, y) \mid y = F_{app}(x)\}$ stands for the graph of F_{app}.

We construct an *iterated function system* (IFS) whose attractor is the graph $Gr(F_{app})$. For $i = 1, 2, \ldots, N$, let $T_i : [0, 1] \times R \to [0, 1] \times R$ be affine transformations of the form:

$$T_i : \begin{bmatrix} x \\ y \end{bmatrix} \mapsto \begin{bmatrix} a_i & 0 \\ b_i & c_i \end{bmatrix} \begin{bmatrix} x \\ y \end{bmatrix} + \begin{bmatrix} d_i \\ e_i \end{bmatrix},$$

where $|c_i| < 1$ is given as a parameter controlling the roughness of the function, and a_i, b_i, d_i and e_i are determined by the constraints

$$T_i(0, y_0) = (x_{i-1}, y_{i-1}),$$
$$T_i(1, y_N) = (x_i, y_i).$$

Choosing the appropriate metrics it can be easily shown that each T_i is a contractive map in the corresponding metric space. Hence, by the fixed point theorem, there exists one and only one function F_{app} satisfying the invariance

$$Gr(F_{app}) = \bigcup_i T_i(Gr(F_{app})), \quad \lim_{n\to\infty} T^n(A) = Gr(F_{app}),$$

where $T = \bigcup T_i$, $T^n = T(T^{n-1})$, and A is a compact set from R^2. Finally, we obtain the resulting graph $Gr(F_{app})$ having a much better resolution in time.

First, we tested the fractal interpolation technique on the time series tree-rings records. For that we formed from original data two time series with sampling intervals 5 and 10 years. Then these time series were used for reconstruction of annual values by means of fractal interpolation technique. The results of comparison of the reconstructed and actual values demonstrate that mean square error of data interpolation for 5-year sampled time series equals to 0.31 (maximal deviation is 1.45), and for 10-year sampled it is 0.44 (maximal deviation is 2.48).

Further we applied fractal interpolation to recovering gaps in original ^{18}O time series and obtained equidistant 5- and 10-year sampled time series of ^{18}O values. For estimation of interrelation between the time series of tree-ring and ice-core records we used the nonlinear correlation method [23]. All available equidistant time series were analyzed, in particular, the 5- and 10-year sampled time series on interval from 5510 BP to 1990 AD and annual data covering the years 818–1987.

4. Denoising of the paleodata time series

While we use the methods of topological dynamics [24], for the estimation of time series interrelation, the task of paleodata time series enhancement becomes very important. This is because the methods give the best results when data has a low level of noise. We used a comprehensive approach to the problem, which is based on the enhancement of Hölder regularity structure of time series. One needs to make no a priori assumption, neither on the nature and parameters of noise nor on the functional relationship between original signal and noise [14,15].

Formally, let $Y = F(X, B)$ be an observed time series, where X is an unknown original signal and B is a noise component, while F corresponds to the functional interrelation between original signal and noise. The primary task is to estimate a local Hölder exponent at each point of Y. Then one can associate Y with its uniquely defined Hölder regularity function α_Y. Afterwards, the next procedure is implemented [15]: $\alpha_Y \to \alpha_Y + \delta \equiv \alpha_{\tilde{X}}$, where $\delta > 0$. Appropriateness of this procedure is confirmed by the fact that for a signal corrupted by noise, its local Hölder exponent is nearly everywhere lower than it is in the case of the original signal. Obtained in such a way, regularity function $\alpha_{\tilde{X}}$ will be used for reconstruction of time series $\tilde{X}$, that is an enhanced copy of the observed time series Y. The next step is the reconstruction of the function $\tilde{X}$ with a given prescribed Hölder regularity $\alpha_{\tilde{X}}$ [25]. This task can be implemented with the help of wavelet analysis [26]. Let $y_{j,k}$ are discrete wavelet coefficients of Y in some orthonormal wavelet basis $\{\varphi_{j,k}\}$, where $\varphi_{j,k}(t) = 2^{j/2}\varphi(2^j t - k)$ and φ is regular enough and has sufficiently many vanishing moments. Then, one can estimate the coarse wavelet Hölder exponent of Y at each point with the help of the next relation [14]

$$|y_{j,k}| \leqslant C 2^{-j(\alpha_Y(k)+1/2)}, \tag{1}$$

where C is a constant and a point k belongs to the support of $\varphi_{j,k}$. The use of orthonormal wavelet basis allows performing the reconstruction in a single way. Starting from the coefficients $y_{j,k}$ of the observations, we modify them to obtain coefficients $\tilde{x}_{j,k}$ that verify the above given relation with the prescribed $\alpha_{\tilde{X}}$ and then reconstruct $\tilde{X}$ using the same basis. In general two conditions must hold true, in particular, (1) enhanced time series X and the observed one Y must be close in the space L^2 [15], i.e.,

$$\|\tilde{X} - Y\|^2 \to \min \tag{2}$$

and (2) the regression of the $\log|\tilde{x}_{j,k}|$ of $\tilde{X}$ above any point k with reference to scale is $-(\alpha(k) + \frac{1}{2})$. Global solution of the $\widehat{X}$ reconstruction task is difficult and demands the evolution algorithm application [15,27]. However, FracLab software allows using simpler variants of the solution with weaker restrictions.

We used the values of $\delta = 1 \div 2$ for all enhanced time series. One can see in Fig. 3 the result of so-called multifractal denoising of the annual ^{18}O data. The effect of time series enhancement is shown in Fig. 4 as a shift of multifractal spectrum $f_g(\alpha)$ towards larger values α, while the form of the spectrum curve remains the

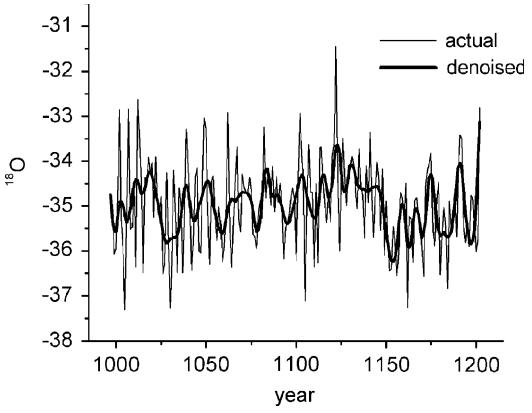

Fig. 3. The original and denoised ^{18}O annual time series.

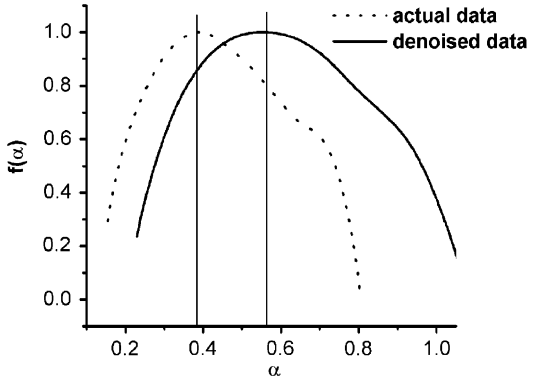

Fig. 4. Large deviation multifractal spectra of original and denoised ^{18}O annual time series.

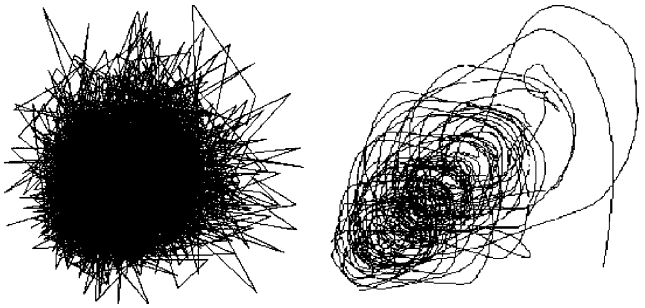

Fig. 5. The phase portraits of original and denoised ^{18}O annual time series.

same. The data enhancement allows extracting the features typical for nonlinear dynamics. This is apparent from phase portraits of time series in Fig. 5 and results in a possibility to estimate, in particular, the correlation dimension of the phase model [24], which is equal to $d_c = 1.8$ for ^{18}O data.

5. Interrelation between the Greenland and Fennoscandian paleoclimatic records

For a proper reconstruction of the paleoclimate it is very important to estimate the interrelation between different proxy data. We investigate proxy data with the help of topological dynamic methods to reveal their interrelationship[24].

Linear relation between nonlinear time series can be absent or very weak. So we used the nonlinear correlation estimation method [28], the idea of which is as follows. Let us construct topological embedding of both time series $\{x_i\}$ and $\{y_i\}$ in R^m by *methods of delay* [24] which simply takes m consecutive elements of the time series directly as coordinates $\mathbf{x}_i$ in the phase space R^m:

$$\mathbf{x}_i = (x_i, x_{i+1}, \ldots, x_{i+m-1})^{\mathrm{T}}, \quad i = 0, 1, 2, \ldots,$$

where embedding dimension m can be estimated, for example, with the help of *correlation integral* method [29]. Such a procedure according to the Takens theorem [30] is "generically" embedding $M \to R^m$ of the genuine attractor of dynamical system $g^n : M \to M$, which produces time series $\{x_i\}$ as scalar projection $M \to R$ of its phase trajectory $g^n(\mathbf{x}_0), n = 0, 1, \ldots$. Thus, there is a diffeomorphism, which maps the genuine attractor of M onto its copy in R^m, if $m \geqslant 2d$, where d is dimension of attractor of dynamical system g^n.

Then, let us denote such reconstructions for the time series as *rec X* and *rec Y*. Then, for *rec X* the number of vector pairs, having distances equal to or less than some positive value ε, is calculated. Next, the number of

ε-close vectors of model *rec Y* is estimated, based on the condition that their synchronous analogs in *rec X* are also ε-close. If the statistical relation between $\{x_i\}$ and $\{y_i\}$ does exist, then it will take place for models *rec X* and *rec Y* also. In this case, the statistics will depend on parameter ε. On the contrary, such a dependence is absent, if the models (and the time series) are statistically independent. Formally, in order to estimate a power of interrelations, the cross correlation ratio is used [23]

$$K_{xy}(\varepsilon) = \sqrt{\frac{\sum_{i\neq j}\|y(i)-y(j)\|^2\Theta(\varepsilon-\|x(i)-x(j)\|)}{\sum_{i\neq j}\Theta(\varepsilon-\|x(i)-x(j)\|)}},$$

where $x(i) = \{x_i, x_{i+\tau}, \ldots, x_{i+(d_x-1)\tau}\}$ and $y(j) = \{y_j, y_{j+\tau}, \ldots, y_{j+(d_y-1)\tau}\}$ are delay vectors of *rec X* and *rec Y* systems, τ is a lag and Θ is the Heaviside function. If systems X and Y are related then one can expect that $\|x(i)-x(j)\| < \varepsilon \Rightarrow \|y(i)-y(j)\| \approx \varepsilon$. If it is not so, K_{xy} does not depend on ε. As a rule, a graph of K_{xy} versus $\log\varepsilon$ is used and rough estimation may be found by means of a slope $s = K_{xy}/\log(\varepsilon)$.

The interdependence of two time series that are proxy indicators of climate fluctuations on large time scales has been studied. The first time series contains the yearly average July temperatures in North Lapland from 5510 BP to 1993 AD [5]. The second time series contains the abundance ratio of oxygen isotope in ice cores of Greenland from 8065 BP to 1987 AD [31]. A topological reconstruction of temperature time series obtained from tree-ring data is taken as the system X. The Y system is a topological reconstruction from oxygen isotope time series. To obtain useful results, denoising procedure has been applied. In order to estimate interrelation on different time scales, the 5- and 10-years sampled time series are also used. Evaluated dependencies of K versus $\ln(\varepsilon)$ are demonstrated in Fig. 6. The slope of the graph's linear intervals enclosed between two vertical lines confirms the presence of the interdependence between X and Y time series. The largest interdependence between X and Y has been found for the annual time series and results in $s = 0.34$. The next values $s = 0.23$ and $s = 0.13$ were estimated for the 5- and 10-year time series, respectively.

As a second approach for examining relationships between two time series we have applied the method of the cross wavelet transform (XWT) [32]. It can be considered to be a natural generalization of bi-spectra or mutual spectra of classic method of the measuring of power spectra. A MatLab software package by the authors [32] for performing XWT can be found at: http://www.pol.ac.uk/home/research/waveletcoherence/. Let

$$W_\psi^X(s,n)[X] = \sqrt{\frac{\delta t}{s}}\sum_{n'=1}^{N} x_{n'}\psi_0\left[(n'-n)\frac{\delta t}{s}\right]$$

be the continuous wavelet transform of a time series $x_n, n = 1, 2, \ldots, N$ with uniform time steps δt and ψ_0 - is the Morlet wavelet, defined as

$$\psi_0(u) = \pi^{-1/4}e^{i\omega_0 u}e^{-(1/2)u^2},$$

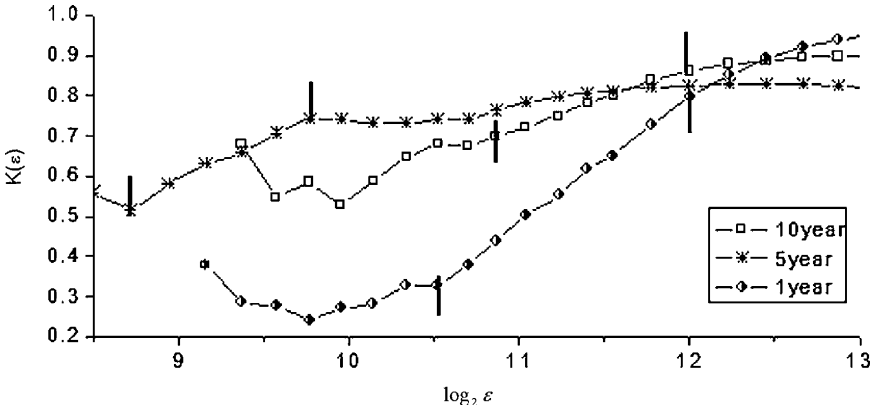

Fig. 6. Estimations of nonlinear interrelation between temperature and oxygen isotope ratio time series for different time scales.

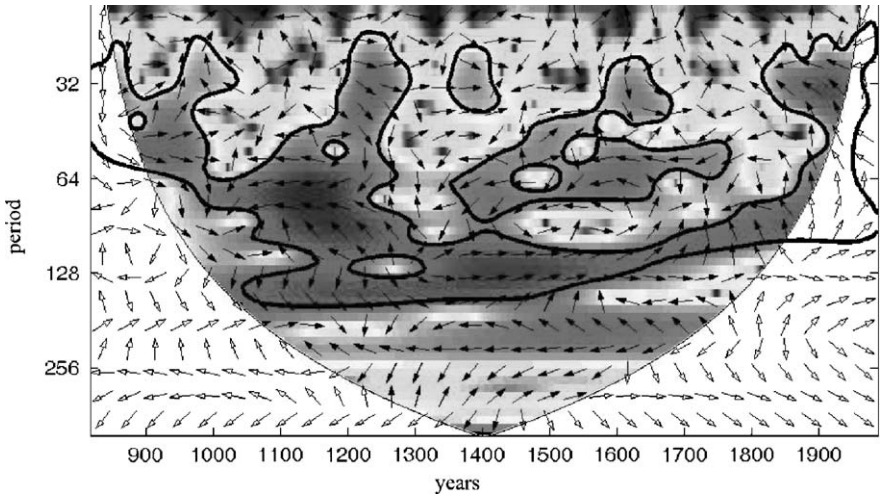

Fig. 7. The cross wavelet transform (XWT) of oxygen isotope ratio and temperature denoised time series.

where ω_0 is a dimensionless frequency and u is dimensionless time. For $\omega_0 = 6$ the Fourier period for the scale s is represented as $\lambda_{\omega t} = 1.03 \times s$. The wavelet power is defined as $|W_n^X(s)|^2$. The complex argument can be interpreted as the local phase.

The XWT of two time series x_n and y_n is defined as $W^{XY} = W^X W^{Y*}$, where $*$ denotes complex conjugation. The theoretical distribution of the cross wavelet power of two time series with background power spectra P_k^X and P_k^Y is given as

$$D\left(\frac{|W_\psi^X(s,n)W_\psi^{Y*}(s,n)|}{\sigma_X\sigma_Y} < p\right) = \frac{Z_v(p)}{v}\sqrt{P_k^X P_k^Y}, \tag{3}$$

where $Z_v(p)$ is the confidence level associated with the probability p for a pdf defined by the square root of the product of two χ^2 distributions.

The XWT shown in Fig. 7 has been constructed for denoised time series of ^{18}O and Finland's temperature T with $\delta = 2$ and $\delta = 1.5$, respectively. The 5% significance level marked in Fig. 7 is calculated using $Z_2(95\%) = 3.999$. The XWT finds regions in time frequency space where the time series show high common power. These regions have been marked by black contours for periods 24–190 years.

6. Conclusion

We have applied the methods of fractal geometry and nonlinear dynamics to analyze the paleoclimatic time series of Finland's temperature and Greenland's ratio of oxygen isotope δ^{18}O records. The results of multifractal formalism have pointed out that paleoclimatic data are characterized by multifractal spectra. This has allowed us to apply fractal interpolation technique to recover missing values in the data by means of iterated function system (IFS). Then, denoising of the data with the help of enhancement of the Holder regularity of the records has provided us with a possibility to preserve nonlinear correlations of the data. This has made them suitable for effective application of nonlinear dynamics methods, especially, to estimate correlation dimension and to reveal interrelation between these climatic indications on the time series of about 8000 years. Since paleoclimatic time series possess well-marked multifractal characteristics, future investigations are likely to be connected with constructions of empirical measures of time series applying the methods of symbolic dynamics. On the other hand, simple models of the multifractal measure based on random iterative function systems (RIFS) can be constructed [16] and a model of the empirical measure can be obtained in a frame of IFS inverse problem [33]. We believe that these models improve our understanding of stochastic dynamics underlying global climatic scenario.

Acknowledgments

Ice-core isotope data used here comes from NOAA paleoclimatology at http://www.ngdc.noaa.gov/paleo. We greatly acknowledge the contributors of this data. The support from INTAS Grant number 2001-0550 is gratefully acknowledged.

References

[1] J.W. Hurrell, Y. Kushnir, M. Visbeck, The North Atlantic oscillation, Science 291 (2001) 603–604.
[2] L.K. Barlow, J.C. Rogers, M.C. Serreze, R.G. Barry, Aspects of climate variability in the North Atlantic sector: discussion and relation to the Greenland Ice Sheet Project 2 high-resolution isotopic signal, J. Geophys. Res. 102 (C12) (1997) 26333–26344.
[3] S.J. Johnsen, et al., The δ^{18}O record along the Greenland Ice Core Project deep ice core and the problem of possible Eemian climatic instability, J. Geophys. Res. Ocean 102 (1997) 26397–26410.
[4] M. Eronen, H. Hyvarinen, P. Zetterberg, Holocene humidity changes in northern Finnish Lapland inferred from lake sediments and submerged Scots pines dated by tree rings, Holocene 9 (5) (1999) 569–580.
[5] M. Eronen, P. Zetterberg, K.R. Briffa, M. Lindholm, J. Merilainen, M. Timonen, The supra-long Scots pine tree-ring record for Finnish Lapland: Part 1, chronology construction and initial references, Holocene 12 (6) (2002) 673–680.
[6] R.W. Aniol, Tree-ring analysis using CATRAS, Dendrochronologia 1 (1) (1983) 45–53.
[7] H.C. Fritts, Tree Rings and Climate, Academic Press, London, 1976.
[8] K.R. Briffa, P.D. Jones, T.S. Bartholin, D. Eckstein, F.H. Schweingruber, W. Karlen, P. Zetterberg, M. Eronen, Fennoscandian summers from AD 500: temperature changes on short and long timescales, Clim. Dyn. 7 (1) (1992) 111–119.
[9] S. Helama, M. Lindholm, M. Timonen, J. Merilainen, M. Eronen, The supra-long Scots pine tree-ring record for Finnish Lapland: Part 2, interannual to centennial variability in summer temperatures for 7500 years, Holocene 12 (6) (2002) 681–687.
[10] P. Mikola, Puiden kasvun vaihteluista ja niiden merkityksesta kasvututkimuksessa. Summary: On the variations in tree growth and their significance to growth studies, Commun. Inst. For. Fenn. 38 (1950) 1–131.
[11] G. Siren, Skogsgranstallen som indicator for klimatfluktuationerna i norra fennoskandien under historisk tid, Commun. Inst. For. Fenn. 54 (1961) 1–66 (Summary in English).
[12] M. Lindholm, Reconstruction of past climate from ring-width chronologies of Scots pine (*Pinus sylvestris* L.) at the northern forest limit in Fennoscandia, Ph.D. Dissertation, University of Joensuu, 1996.
[13] M.F. Barnsley, Fractal functions and interpolation, Constr. Approx. 2 (1986) 303–329.
[14] J. Lèvy Vèhel, E. Lutton, Evolutionary signal enhancement based on Holder regularity analysis, EVOIASP2001, Lecture Notes in Computer Science, vol. 2038, Springer, Lake Como, Italy, 2001.
[15] J. Lèvy Vèhel, Signal and enhancement based on Holder regularity analysis, IMA Volumes in Math. Appl. 132 (2002) 197–209.
[16] K.J. Falconer, Fractal Geometry, New York, Wiley, 2003.
[17] R. Riedi, in: Doukhan, Oppenheim, Taqqu (Eds.), Multifractal Processes Long Range Dependence, Birkhauser, Basel, 2002, pp. 625–715.
[18] T.C. Halsey, M.H. Jensen, L.P. Kadanoff, I. Procaccia, B.I. Schraiman, Fractal measures and their singularities: the characterizations of strange sets, Phys. Rev. A 33 (1968) 1141–1151.
[19] S. Jaffard, Multifractal formalism for functions, SIAM J. Math. Anal. 28 (1997) 944–970.
[20] R. Riedi, An improved multifractal formalism and self-similar measures, J. Math. Anal. Appl. 189 (1995) 462–490.
[21] R. Riedi, I. Scheuring, Conditional and relative multifractal spectra, Fractals 5 (1997) 153–168.
[22] J. Lèvy Vèhel, Numerical Computation of the Large Deviation Multifractal Spectrum, //URL: ⟨http://www-rocq.inria.fr/fractales⟩.
[23] A. Čenis, G. Lasiene, K. Pyragas, Estimation of interrelation between chaotic observables, Physica D 52 (1991) 332–337.
[24] T. Sauer, J.A. Yorke, M. Casdagli, Embedology, J. Stat. Phys. 65 (1991) 579–616.
[25] J. Lèvy Vèhel, K. Daoudi, Y. Meyer, Construction of continuous functions with prescribed local regularity, Constr. Approx. 014 (1998) 349–385.
[26] S.t. Mallat, A Wavelet Tour of Signal Processing, Academic Press, New York, 1999.
[27] L. Karimova, E. Kuandykov, N. Makarenko, Genetic algorithm for signal enhancement, Nucl. Instrum. Methods Phys. Res. A 534 (2004) 170–174.
[28] P. Schneider, P. Grassberger, Studying attractor symmetries by means of cross-correlation sums, Nonlinearity 10 (1997) 749–762.
[29] P. Grassberger, I. Procaccia, Measuring the strangeness of strange attractors, Physica D 9 (1983) 189–208.
[30] F. Takens, Detecting strange attractors in turbulence, Lecture Notes in Math. 898 (1981) 366–381.
[31] M. Stuiver, P.M. Grootes, T.F. Braziunas, The GISP2 $\delta^{18}O$ climate record of the past 16,500 years and the role of the sun, ocean and volcanoes, Quat. Res. 44 (1995) 341–354.
[32] A. Grinsted, J.C. Moore, S. Jevrejeva, Application of the cross wavelet transform and wavelet coherence to geophysical time series, Nonlinear Process. Geophys. 11 (2004) 561–566.
[33] M.F. Barnsley, V. Ervin, D. Hardin, J. Lancaster, Solution of an inverse problem for fractals and other sets, Proc. Natl. Acad. Sci. USA 83 (1986) 1975–1977.